

Review

Fifty Years After the Discovery of the First Stellar-Mass Black Hole: A Review of Cyg X-1

Jiachen Jiang ^{1,2} 

¹ Department of Physics, University of Warwick, Gibbet Hill Road, Coventry CV4 7AL, UK; jiachen.jiang@warwick.ac.uk

² Institute of Astronomy, Madingley Road, Cambridge CB3 0HA, UK

Abstract: Around 50 years ago, the famous bet between Stephen Hawking and Kip Thorne on whether Cyg X-1 hosts a stellar-mass black hole became a well-known story in the history of black hole science. Today, Cyg X-1 is widely recognised as hosting a stellar-mass black hole with a mass of approximately 20 solar masses. With the advancement of X-ray telescopes, Cyg X-1 has become a prime laboratory for studies in stellar evolution, accretion physics, and high-energy plasma physics. In this review, we explore the latest results from X-ray observations of Cyg X-1, focusing on its implications for black hole spin, its role in stellar evolution, the geometry of the innermost accretion regions, and the plasma physics insights derived from its X-ray emissions. This review primarily focuses on Cyg X-1; however, the underlying physics applies to other black hole X-ray binaries and, to some extent, to AGNs.

Keywords: binaries; black holes; X-ray observations; accretion; plasma physics; accretion

1. Cyg X-1: The First-Ever Discovered Stellar-Mass Black Hole

Cyg X-1 is one of the brightest persistent X-ray sources in the sky, with an X-ray flux ranging from 0.2–2 Crab (see Figure 1 for an image of Cyg X-1). It was the first system widely believed to host a stellar-mass black hole (BH) after the work of Bolton [1], Webster and Murdin [2]. The discovery of Cyg X-1 as an X-ray source dates back even further, to 1964 [3]. The famous bet between Stephen Hawking and Kip Thorne in 1974 on the existence of a BH in Cyg X-1 [4] has since become a celebrated story in the scientific history of BHs. Fifty years on, advanced X-ray telescopes have enabled numerous discoveries across various aspects of X-ray binaries like Cyg X-1. In this review, I summarise some of the latest findings, focusing on X-ray observations.

The X-ray emission from Cyg X-1 primarily originates from the accretion of powerful stellar winds from its super-giant companion star [5]. A parallax study by Miller-Jones et al. [6] has precisely measured the distance to Cyg X-1 at 2.2 ± 0.2 kpc, providing a well-constrained BH mass of $21 \pm 2 M_{\odot}$ and a companion star mass of $40 M_{\odot}$. This massive companion star places Cyg X-1 among the high-mass X-ray binaries (HMXBs). Currently, there are only a small number of known BH HMXBs, as listed in Table 1, among which the nature of the compact object in MWC 656 is still debated [7]. The rarity of BH HMXBs is largely due to selection effects: donor stars in low-mass X-ray binaries (LMXBs) typically have ages of $\geq 10^9$ years, whereas those in HMXBs are much younger, with ages of $\leq 10^6$ years. Consequently, the likelihood of observing a BH LMXB is higher than finding a BH HMXB. Cyg X-1 stands out as a unique example with the most massive BH and the second most massive donor star, following M33 X-7.

This review is structured around three major topics. First, I explore the role of Cyg X-1 in stellar evolution, focusing on its near-maximal BH spin, as measured through relativistic disk reflection and thermal continuum emission. I discuss the implications of these measurements for theories of stellar evolution. Second, I focus on accretion physics, emphasising the innermost accretion geometry, particularly in light of recent X-ray polarisation



Citation: Jiang, J. Fifty Years After the Discovery of the First Stellar-Mass Black Hole: A Review of Cyg X-1. *Galaxies* **2024**, *12*, 80. <https://doi.org/10.3390/galaxies12060080>

Academic Editor: Christian Corda

Received: 15 September 2024

Revised: 9 November 2024

Accepted: 12 November 2024

Published: 21 November 2024



Copyright: © 2024 by the author. Licensee MDPI, Basel, Switzerland. This article is an open access article distributed under the terms and conditions of the Creative Commons Attribution (CC BY) license (<https://creativecommons.org/licenses/by/4.0/>).

measurements. Lastly, I cover plasma physics, focusing on high-energy pair plasma inferred from hard X-ray observations of the corona and photo-ionised plasma inferred from soft X-ray observations of the accretion disk in Cyg X-1. Although this review centres on Cyg X-1, many of the models discussed extend to other X-ray binaries or even active galactic nuclei (AGNs).

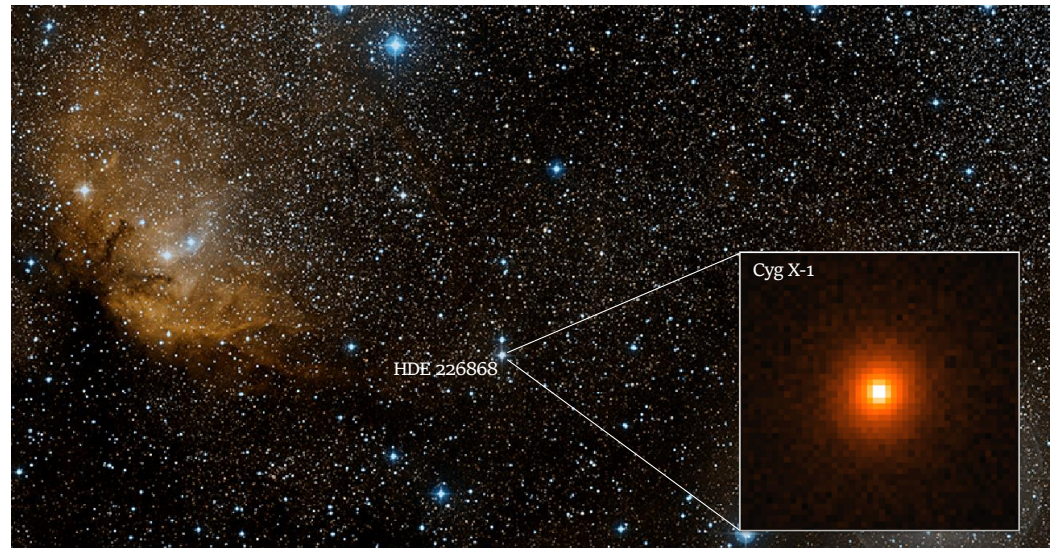


Figure 1. The ESO Digital Sky Survey optical image of the sky area of 60 by 30 arcmins around Cyg X-1. The blue dots in this image show the luminous young blue stars. One of them, the supergiant star HDE 226868, has an invisible BH companion. The accretion process from the star to the BH radiates significant X-ray emission. The zoom-in image shows the *ROSAT* image of the corresponding X-ray source Cyg X-1. The cloud to the left of the image is Sh2-101, a nearby H II region emission nebula located in the constellation Cygnus.

Table 1. Known BH HMXBs in the local group. Values are from Miller-Jones et al. [6], van den Heuvel [8]. Note that the nature of the compact object in MWC 656 is still debated (e.g., [7]).

Name	P (Days)	M_2 (M_\odot)	M_{BH} (M_\odot)
Cyg X-1	5.6	40^{+8}_{-7}	21 ± 2
LMC X-1	3.9	31.8 ± 3.5	10.9 ± 1.4
LMC X-3	1.7	3.6 ± 0.6	7 ± 0.6
MWC 656	≈ 60	≈ 13	4.7 ± 0.9
M33 X-7	3.45	70 ± 7	15.6 ± 1.5

2. Cyg X-1 as the Laboratory for Stellar Physics

2.1. Measure the Spin of the Black Hole in Cyg X-1

The no-hair theorem posits that all stationary BH solutions can be completely characterised by only three independent parameters: mass (M), angular momentum (J), and negligible electric charge in an astrophysical expectation. The angular momentum or spin (J/M^2) of a BH is particularly significant as it encodes information about the BH's formation history (e.g., by mergers or accretion). Spin may theoretically play a critical role in powering jets that allow BHs to influence their surroundings. Most notably, high spin can produce extreme relativistic effects, such as frame-dragging, giving us a unique opportunity to test gravitational theories in the strong-gravity regime. The further implications of BH spin measurements can be found in Reynolds [9], which I will not expand upon here.

There are two established methods for measuring the spin of a BH—the relativistic reflection [10,11] and continuum fitting (CF, [12,13]) methods. Both of these techniques work in a similar manner: by measuring the light from the innermost regions of the accretion disk, we attempt to determine where it terminates outside the BH and, from that, infer the spin using the simple correlation between the innermost stable circular orbit and BH spin. The CF method measures the temperature and luminosity of the accretion disk spectrum, which is hotter and brighter near the BH. The reflection method instead measures how the fluorescent iron line in the X-ray spectrum, produced by X-ray reflection from the inner accretion disk, is distorted by the spacetime close to the BH, thereby inferring the inner radius.

Cyg X-1 was the first stellar-mass BH to be confirmed, and therefore, it has been extensively studied in the context of BH spin measurements. The spin of Cyg X-1 has been measured to be higher than 0.95 using the continuum-fitting (CF) method [14–17]. Relativistic disk reflection modelling has yielded spin values higher than 0.9 [18–22]. Although alternative coronal geometries could introduce systematic uncertainties, the spin value remains high. For instance, Krawczynski and Beheshtipour [23] considered a cone-shaped coronal region illuminating the accretion disk and still found a disk spin of at least 0.86.

2.2. The Missing Links Between Cyg X-1 and Gravitational Wave Binaries

The donor stars in HMXBs were believed to be massive enough to form a compact object, e.g., a neutron star (NS) or a BH, making them prime candidates for the progenitors of compact object binaries, as in the gravitational wave (GW) sources (e.g., [24]). However, the inconsistency between their BH spin distributions was soon noticed by the community (e.g., [25,26]). Accretion after BH formation was proposed to explain the high BH spins in BH HMXBs. However, since the accretion process cannot occur for longer than the lifetime of the donor [6], the observed close-to-maximum spin of Cyg X-1 would require a persistent super Eddington accretion process [27], but Cyg X-1 is only observed to accrete with $2 \times 10^{-7} M_{\odot} \text{ yr}^{-1}$ now. The actual accretion time may be even shorter than the age of the donor star, making the spin-up-due-to-accretion scenario more challenging [28].

The spin discrepancy between Cyg X-1 and GW binary BHs motivated a recent development in a modified relativistic disk model, including a ‘warm’ corona for the X-ray data of Cyg X-1 that may lead to a lower inferred BH spin [29], but such a development does not show significant statistical improvement in data fitting compared to the previous models (e.g., [14]). The condition of a ‘warm’ corona in Cyg X-1, similar to the ones proposed for supermassive BH accretion disks in AGNs with dramatically different BH disk temperatures and luminosities [30], has yet to be examined [31].

2.3. The Origin of the High BH Spin in Cyg X-1

In this review, I would like to highlight the large uncertainty on whether the known population of BH HMXBs can contribute significantly to the observed GW binary BHs and whether they make comparable systems.

Take Cyg X-1 as an example. Neijssel et al. [32] conducted a population synthesis test based on the donor star and BH mass measurements in Miller-Jones et al. [6]. They found that Cyg X-1 will have only a 7% chance of forming a BH-NS binary and remaining bound after the NS natal kick. After revising mass transfer models, Neijssel et al. [32] found the probability of Cyg X-1 forming a binary BH within a Hubble time is 4%. Similar conclusions were achieved for the other BH HMXB LMC X-1 [33].

The close-to-maximum spin of Cyg X-1 inferred by the X-ray data likely results from the angular momentum of the progenitor star’s core instead of purely due to accretion. For example, Gallegos-Garcia et al. [34] found that high-spin BH HMXBs can form through main sequence mass transfer from the BH progenitor to the secondary star (Case A mass transfer). The core of the progenitor is tidally locked and, hence, rapidly rotating, which can produce high BH spins [35]. Evidence of such a stellar evolution pathway includes the observed enhanced nitrogen abundances in the donor star of Cyg X-1 [36]. For the

Case-A mass transfer model, mass is transferred from deep layers of the progenitor star, reprocessed from the CNO cycle (for carbon–nitrogen–oxygen) and is thus nitrogen rich. This evolution pathway is also supported by the low orbital eccentricity of Cyg X-1 [6].

Alternatively, it was also suggested that slow ejecta from a failed supernova that formed the BH could interact with the companion and be torqued, increasing their angular momentum before falling back onto the newly formed BH [37]. Hydrodynamical simulations in Schröder et al. [38] show that such a spin-up process is consistent with some of the GW binary BHs at the higher end of the spin distribution, but whether it is sufficient to spin up to close-to-maximum spin as in Cyg X-1 remains a question.

Furthermore, the significant BH mass difference between GW binary BHs and observed BH HMXBs also indicates their fundamental difference. The primary BH mass distribution compiled from GW observations peaks around $35M_{\odot}$ [39]. No observed BH HMXBs are close to this mass limit (see Table 1).

Suppose that Cyg X-1 may not represent the best candidate progenitor for GW binary BHs due to significantly different BH masses and spins. Can we extend such a conclusion to other HMXBs that have yet to be detected? Liotine et al. [40] used population synthesis calculations and applied realistic X-ray and GW observational limits of *Chandra* and advanced LIGO. They found, due to observational selection effects, only a 3% probability of a detectable HMXB host BH of $>35 M_{\odot}$. The probability of finding a HMXB forming a binary BH system as the GW sources within a Hubble time is only 0.6%. Therefore, unsurprisingly, the currently observed BH HMXBs, like Cyg X-1, do not resemble the features of GW binary BHs.

2.4. Black Holes in the Mass Gap

The findings of short-period, high-BH mass GW binaries are intriguing as they surpass the masses predicted by most stellar evolution models and exceed the known stellar-origin BHs in our galaxy: stars of an initial mass of higher than $30 M_{\odot}$, as the donor star of Cyg X-1, are expected to lose significant mass and only produce BHs of $<20 M_{\odot}$ [41,42].

Isolated stellar-mass BHs with masses of a few tens of solar masses, formed through typical stellar evolution, are challenging to detect. Gravitational microlensing techniques can be employed to identify these isolated BHs (e.g., [43–45]), and some candidates have been identified with masses in the range of $10\text{--}100 M_{\odot}$ [46].

A prevailing hypothesis proposes that these high-mass stellar-mass BHs bound in a binary system, such as those detected as GW sources, are remnants of massive, metal-poor stars. Low metallicity leads to notably less mass loss due to metallicity-dependent winds during the star's lifetime [41]. Additionally, the reduced metallicity decreases the radius of the progenitor, lowering the likelihood of mergers during the common-envelope phase [47,48]. Finally, the higher BH mass resulting from low-metallicity progenitors corresponds to weaker natal kicks at formation, which increases the chances of preserving the binary system as a bound pair [49]. This scenario is particularly supported by the new discovery of a $32.7 \pm 0.8 M_{\odot}$ BH in a binary system with a period of 11.6 years, identified through *Gaia* astrometric data [50]. The broad-band photometric and spectroscopic data also confirm the existence of a very metal-poor, old companion star at a distance of 590 pc, suggesting that metal-poor environments may play a crucial role in the formation of such massive BHs [50].

3. Cyg X-1 as the Laboratory for Accretion Physics

3.1. The Persistently High Radiative Efficiency

Unlike many other BH transients, Cyg X-1 has never reached the quiescent state since its discovery in the X-ray band. Figure 2 shows the X-ray brightness of Cyg X-1 as measured by *MAXI*. The *MAXI* X-ray count rate alternates between high and low states, both of which exhibit significant variability. This behaviour results in a double-peaked log-normal distribution, as shown in Panel C. The two peaks correspond to different spectral states: the soft state, marked in grey, where the *MAXI* count rate is high and the hardness

ratio is low; and the hard state, marked in purple, where the *MAXI* count rate is low and the hardness ratio is high. As the X-ray flux decreases, the hardness ratio correspondingly increases. This creates two distinct clusters in the hardness-intensity diagram (HID) shown in Panel D of the same figure. During transitions from the hard to soft state, Cyg X-1 briefly passes through an intermediate state. Different X-ray spectral states were realised soon after the X-ray data of Cyg X-1 became available (e.g., [51]).

It is important to note that, due to historical reasons, the X-ray HIDs of transients are typically presented using X-ray count rates. However, these count rates do not accurately reflect the true X-ray flux, as the photon-collecting area of the telescope varies across different energy bands. Despite the fact that the *MAXI* count rate appears lower in the hard state, the actual X-ray luminosity is not significantly reduced. This is because the spectrum is harder, meaning each photon carries more energy. For a more detailed discussion on instrument-dependent state transitions, see Grinberg et al. [52].

Panel E illustrates the quasi-simultaneous *Suzaku* and *NuSTAR* spectra of Cyg X-1 during the soft, intermediate, and hard states, corresponding to the three highlighted positions in the HID shown in Panel D. The Eddington ratios of Cyg X-1 during these observations were measured to be around 1%, with values ranging from 0.62% to 1.72% (e.g., [53]), corresponding to, as König et al. [54] demonstrates, the lower end of the classical q-shaped HID typically observed in LMXBs. The persistently high accretion rate is likely a consequence of the BH being embedded in the stellar winds of its massive donor star. Similar persistent X-ray emission is observed in other BH HMXBs, such as LMC X-1 and LMC X-3.

Cyg X-1 has not been observed in a quiescent state, unlike many BH transients in LMXBs [55], where low accretion rates lead to the formation of a radiatively inefficient, optically thin flow due to the importance of viscous heating advection (e.g., [56]). In contrast, the presence of significant disk thermal and reflected emissions in both the soft and hard states of Cyg X-1 suggests the existence of an optically thick accretion disk extending close to the innermost stable circular orbit (e.g., [14,20]).

Extending the discussion of accretion flow structures from Cyg X-1 to a broader range of BH XRBs, the precise Eddington ratio at which the transition occurs—from an optically thin, radiatively inefficient, advection-dominated accretion flow to an optically thick, radiatively efficient, geometrically thin accretion disk, as observed in Cyg X-1—is still debated within the observational community, though it is generally thought to lie between 0.1% and 10% of the Eddington luminosity. For example, some studies, such as Plant et al. [57], have identified a significantly truncated, optically thick accretion disk at a few tens of gravitational radii in GX 339–4 at an Eddington ratio of a few percent. In contrast, other groups report an optically thick disk extending to the innermost stable circular orbit for the same object at a similar luminosity [58]. The formation of an optically thick accretion disk may depend on the specific environment of each object. However, Cyg X-1 is distinctive in that it remains around 1% of the Eddington luminosity, serving as a unique laboratory for accretion studies—a topic I will expand on in a later section.

Future high-resolution X-ray spectroscopy, such as that from *XRISM* equipped with microcalorimeters, will be crucial in revealing the nature of accretion disks through observations in the iron emission band. *XRISM* has already demonstrated remarkable spectral measurement capabilities, disentangling multiple iron line emission components when used jointly with CCD-resolution data (e.g., [59,60]). As of this writing, analysis of the *XRISM* observations of Cyg X-1 is ongoing.

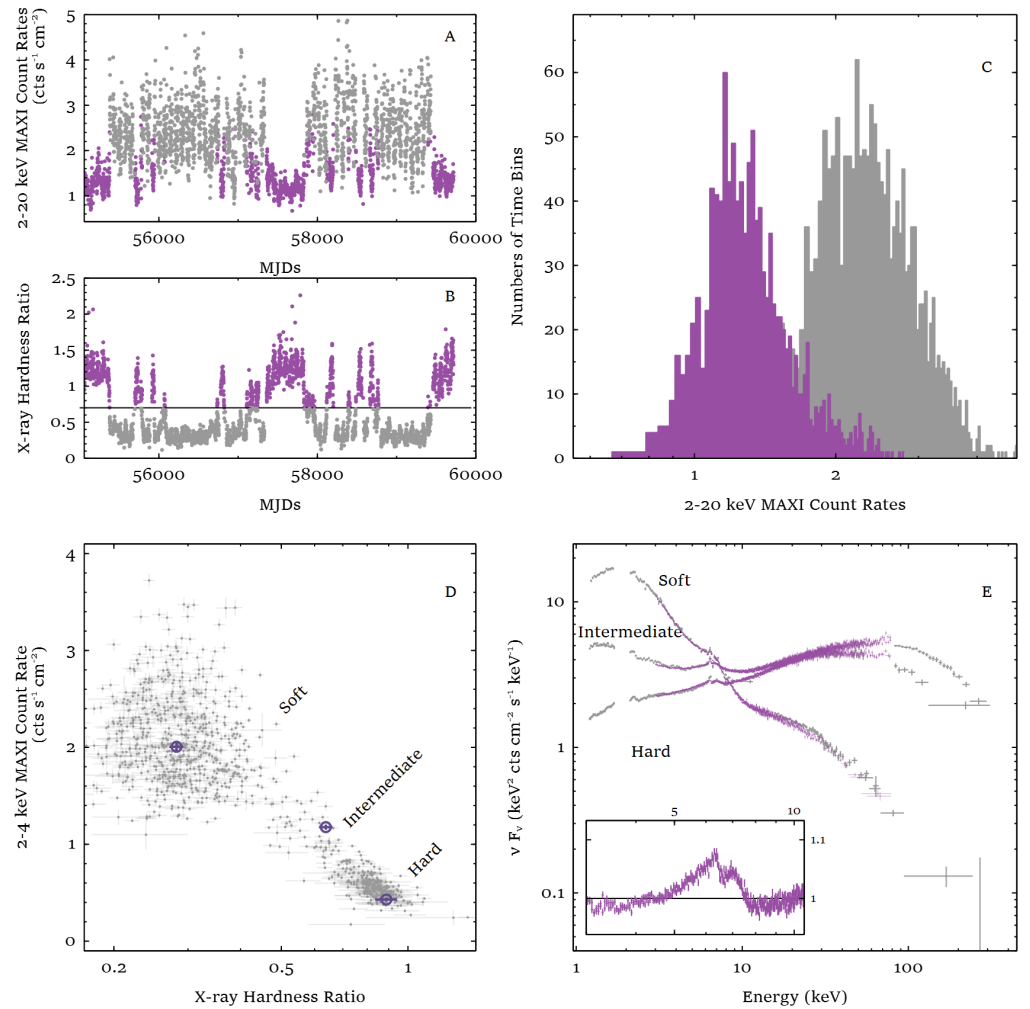


Figure 2. (A,B): *MAXI* 2–20 keV daily light curve and hardness ratio of Cyg X-1. (C): The distribution of *MAXI* X-ray count rates of Cyg X-1 shows a double-peaked log-normal distribution. The purple (grey) distribution corresponds to the hard (soft) state. (D): *MAXI* hardness-intensity diagram. (E): Quasi-simultaneous *NuSTAR* and *Suzaku* spectra of Cyg X-1 in the soft, intermediate and hard states. Their corresponding hardness ratio was marked by purple in Panel D. The inset window shows the zoom-in of the hard state spectrum of Cyg X-1, demonstrating significant evidence of relativistic disk Fe K emission lines. Detailed analyses of these spectra can be found in Tomsick et al. [19], Parker et al. [20], Walton et al. [22], Tomsick et al. [53].

3.2. The Accretion Geometry of Cyg X-1

Coronal geometry: the geometry of the X-ray Comptonisation region—where disk seed photons are Compton-upscattered by an electron cloud with an optical depth of $\tau \approx 0.5\text{--}2$ [61,62], often referred to as the corona—remains a topic of debate. Despite the uncertain geometry, the size of the corona is known to be small in various accreting BH systems, including stellar-mass BH transients and AGNs, as evidenced by reverberation and gravitational lensing studies [63–66]. Additionally, the steep emissivity profile of the accretion disk also suggests a compact corona [67]. The latter was investigated in detail for Cyg X-1 using the *Suzaku* data [18]. The emissivity profile of the disk in Cyg X-1 is consistent with the model for a compact coronal region with a size of $5\text{--}7 r_g$.

The geometry of the corona is closely linked to the question of its origin, making it essential to constrain the corona’s geometry through observations. Historically, the “lamp-post” geometry, in which a point source is located along the BH’s spin axis, has often been assumed when modelling the X-ray spectra and timing properties of accreting BH tran-

sients, including Cyg X-1 (e.g., [20]). This approximation is based on theories suggesting a jet-based origin for the corona [68–70].

However, the “lamppost” model should not be taken too literally; it is merely a simplification representing a very compact coronal region near the BH. We often adopt this point-like geometry because it is computationally convenient. For example, setting the initial condition along the spin axis in relativistic ray-tracing calculations is far simpler than modelling more complex geometries. Nonetheless, several alternative geometries have been proposed, such as a spherical or outflowing jet-shaped corona [71], sandwich or wedge layers above the disk [72,73], and thick accretion flows within a truncated disk [74].

Surprisingly, shortly after the launch of *IXPE*, Cyg X-1 was found to exhibit a higher-than-expected polarisation degree in the hard state. While a low polarisation degree of less than 1% was anticipated from the corona, observations in the 2–8 keV band revealed a polarisation degree of around 4% [75]. Moreover, the polarisation angle aligns with the AU-scale jet position angle of Cyg X-1 in the sky, as well as with the pc-scale radio lobes [76]. This suggests that the corona may be extended over the plane of the accretion disk, assuming the polarisation originates entirely from the corona rather than the jet.

However, a horizontally extended coronal region does not fully explain the unexpectedly high polarisation degree. Krawczynski et al. [75] proposed that if the corona is a layer on the disk with the same inclination as the disk, then the inner disk must have a significantly higher inclination than the binary’s orbital plane (e.g., around 30° [6]). Previous disk reflection spectral models indeed suggested a possible misalignment of around 13° [19].

Alternatively, if the corona is outflowing at a relativistic velocity of $\geq 0.4c$, the angular distribution of seed photons would be significantly different in the plasma’s rest frame. This would result in a higher polarisation degree for the outgoing scattered radiation without the need for a high inclination angle to explain the data [77].

It is crucial to consider the implications of such high velocities within the corona. As discussed in a later chapter, the compact, hot corona is primarily composed of pair plasma. A key question remains whether such a high velocity might exceed the equilibrium velocity of the pairs, the exact value of which depends on the optical depth of the pair plasma and is estimated to be around 0.3–0.4 c for the condition similar to Cyg X-1 [78]. Additionally, a highly outflowing corona would result in a significantly lower disk reflection fraction compared to a static corona model [79,80] because of the beaming effects. A fully consistent disk reflection model for the spectral and polarisation data of Cyg X-1 that incorporates the consistent coronal geometry has yet to be developed.

Last but not least, it is important to acknowledge two key points. First, the geometry of the corona may be highly source-dependent. For example, if the corona is magnetised (e.g., [81,82]) or regulated by radiation, both mechanisms depend on the specific model used or the target observed, making it challenging to draw broad conclusions from a small sample of sources. Second, due to the limitations of current observational methods, we are still in the phase of testing different geometries by making assumptions within models. Nature often behaves in unexpected ways, so the scientific community must remain open-minded. While testing specific geometries, it is crucial not to exclude other possibilities or the potential combination of simple geometries, e.g., a disk-shaped lamppost corona that corotates with the disk of Cyg X-1. An effort in this direction is being developed (Bambi, in private communication). The size of the corona is not constrained by polarisation data but can well be by timing and spectral data. A joint analysis of timing and spectral and polarisation data has yet to be complete.

Links to the jet: the explanations above do not entirely rule out a jet origin for the 2–8 keV polarisation observed in Cyg X-1. Dexter and Begelman [83] proposed that a weakly polarised seed emission, such as that expected from a standard lamppost corona or the disk, could be Compton-upscattered by cold electrons¹ in the jet, which is the so-called bulk Comptonisation model. A highly polarised scattered emission can result from this interaction because relativistically moving electrons have a higher scattering cross-section for anisotropic radiation beamed in the direction of their motion [84].

To understand Cyg X-1 in the hard state, the community ought to explore synergistic opportunities. Moving on to other wavelengths, the high polarisation degree of Cyg X-1 in the soft Gamma-ray band, e.g., $>20\%$ [85], is likely due to the synchrotron emission from the jet, which is prominent in the hard state, as indicated by its strong radio emission, and typically quenched in the soft state. The jet's soft gamma-ray emission overlaps with the X-ray Comptonisation component at lower energies and is associated with the radio jet. These features align with the multi-component emission processes predicted by compact jet models, such as those proposed by Markoff et al. [70]. A recent comprehensive study of the multi-wavelength polarisation properties of Cyg X-1 by Russell and Shahbaz [86] demonstrated that the spectrum and polarisation are consistent with a compact jet dominating the radio to the infrared range and contributing to the MeV tail.

Intriguingly, *INTEGRAL* observations found a polarisation angle of 40° above 230 keV [85,87], which is 60° different from the angles observed in optical, infrared, 2–8 keV bands as well as the radio jet orientation [86,88]. *AstroSAT* found an almost 90° difference between the 100–380 keV energy band and radio jet orientation [89]. A similar deviation between radio jet orientation and soft gamma-ray polarisation angles was also discovered in the hard state observations of other BH XRBs (e.g., [90]). This discrepancy suggests possibly complex magnetic field structures or multiple electron populations within the jet. To fully understand the hard state of Cyg X-1, it is essential to develop consistent multi-wavelength models that account for the jet's contribution.

Disk geometry: Steiner et al. [91] reports that *IXPE* measurements of Cyg X-1 in the soft state show a polarisation angle consistent with the radio jet orientation. The polarisation degree is two percent lower than in the hard state. Similar conclusions were found in Jana and Chang [92]. Similar to the hard state, the polarisation degree in the 2–8 keV band increases with energy. Comparable results have been observed in the soft states of other LMXBs [93–97].

The very high polarisation degree observed in the soft state, dominated by disk thermal emission, suggests that the classical standard disk model, which assumes a semi-infinite, free-electron scattering atmosphere [98], may no longer be applicable. Additionally, general relativity predicts a decrease in polarisation degree with increasing energy, which contrasts with observations of Cyg X-1 and other objects, such as 4U 1630–47 [94].

One possible solution to achieve such a high polarisation degree, proposed by Ratheesh et al. [93], involves a scattering atmosphere in 4U 1630–47 with an outflow velocity of 0.5 c —similar to the velocity assumed for the hard-state outflow (Notably, this outflow in the soft state involves particles, while the hard state involves a pair plasma outflow). In such a disk model, absorption within the outflowing atmosphere results in a high degree of polarisation parallel to the disk surface. While this model may not align with the observed polarisation angle for Cyg X-1, it could apply to other objects with different polarisation orientations, such as 4U 1630–47.

An alternative method to achieve higher polarised flux is through reflection due to disk self-irradiation, which is more likely the case for Cyg X-1 [91]. This model has also been successful for other objects (e.g., [96]). In this scenario, harder X-rays from a hotter region of the accretion disk that is closer to the BH are more likely to be reflected back to the disk. This reflection naturally increases the polarisation degree with energy, consistent with the observations of Cyg X-1. It is important to note that the strength of returning radiation strongly depends on the BH spin. Only systems with extremely high BH spin, such as Cyg X-1, can generate significant polarisation through a self-irradiated disk. This is consistent with previous spectral measurements of the BH spin in Cyg X-1 (see Section 2.1).

However, it is crucial to note that the polarisation degree of a self-irradiated disk depends on the disk geometry. The assumption of a razor-thin disk model may be valid for Cyg X-1, given its consistently low luminosity (less than 10% of its Eddington luminosity). This assumption may be less applicable to other BH transients (e.g., [99,100]), where luminosity can commonly peak around the Eddington limit in the soft or ultra soft states.

3.3. Fast X-Ray Variability

Variability: the study of variability on short timescales is often conducted in the Fourier frequency domain using the power spectral density (PSD) spectra.

The hard state of Cyg X-1 exhibits broad-band noise that can be decomposed into multiple Lorentzian components [54,101,102]. Occasionally, some very high-frequency Lorentzian components are required to fit the PSD [102,103], although they do not always persist consistently. These Lorentzian components remain at the same Fourier frequency, but their strength varies with energy: harder X-rays show more variability than the softer X-rays. For instance, *NICER* measured the root-mean-square (RMS) variability, integrated over all Fourier frequencies, to be 19% in the 0.5–1 keV band and a higher value of 30% in the 5–8 keV band [54].

Some of the extreme variability observed in the hard state is likely linked to the same processes responsible for the typical X-ray variability seen during smaller flares [104]. This suggests that the powerful flares in the low/hard state are part of the same variability mechanism driving the more frequent, lower-amplitude fluctuations. This view aligns well with the exponential model, which predicts a lognormal distribution of fluxes [105].

In the intermediate state, the PSD of Cyg X-1 reveals a broad Lorentzian component, which predominantly influences the hard X-ray band above 3 keV. In the soft X-ray band, where disk thermal emission dominates, the RMS variability is significantly lower, although the PSD retains a similar shape [54].

In the soft state, the variability of Cyg X-1 exhibits typical red noise behaviour. Similar to the intermediate state, the RMS variability increases from 7% in the 0.5–1 keV band to 30% in the 5–8 keV band [106,107]. The overall RMS variability across the 0.5–10 keV range is around 10% [108], which is substantially higher than that of most LMXB transients in the soft state, where the RMS is typically below 1%, such as in MAXI J1820 + 070 [109].

Several of the previous studies have demonstrated that the X-ray timing characteristics of other accreting compact objects exhibit a linear relationship between their RMS variability and average flux across various timescales (e.g., [110]). This relationship suggests non-stationarity in the light curves, where the level of instantaneous variance is not constant but instead scales with the longer-term flux averages. Uttley et al. [104] highlight that these properties imply a lognormal distribution of instantaneous flare strengths. This can be explained if the observed variations are not the result of a superposition of independent shots but rather due to accretion rate fluctuations occurring at all locations within the accretion flow. These fluctuations propagate inward, coupling perturbations at different radii. Interestingly, a similar “RMS–flux relation” has been observed in other systems, such as narrow-line Seyfert galaxies [111], suggesting that this relation may universally constrain the fluctuating conditions of hot plasmas.

Coherence and lags: Cyg X-1 exhibits complex behaviour in terms of coherence and time lags, which vary depending on the choice of energy bands and Fourier frequencies. I will not demonstrate the intricate details in this review. Readers may instead refer to the series of work in the past decades [54,102,106,112,113]. There are numerous uncertainties in their interpretations: for instance, while lags are well documented in the soft state, where the disk thermal emission dominates the X-ray band [52,54], the origin of these lags remains unclear.

In the hard and intermediate states, where RMS variability is higher and the coherence between soft and hard X-ray variability is greater than in the soft state, both hard and soft lags are detectable and much better understood than in the soft state. The hard X-ray lag, relative to the soft X-rays, increases with energy, supporting propagating fluctuation models [114]. While the emission might originate primarily from the innermost regions, the variability likely arises throughout the entire accretion flow. In particular, Arévalo and Uttley [115] showed such a propagation model for Cyg X-1 in great detail.

The X-ray spectra of Cyg X-1 across various accretion states exhibit substantial evidence of disk-reflected emission, with the most prominent feature being relativistic broad Fe K emission lines spanning the 6–7 keV range. Interestingly, no clear iron line lag fea-

tures as in LMXBs (e.g., [64]) have been detected in archival observations of Cyg X-1 from *RXTE* [116], *NICER* [54], or *Insight-HXMT* [107], likely due to the limited reflection strength in the iron emission band. However, significant soft lags have frequently been observed [54], which have been interpreted as the light-crossing time between the hard X-rays from the corona and the soft X-ray photons from the disk, similar to findings in other systems [117,118].

4. Cyg X-1 as the Laboratory for High-Energy Plasma Physics

4.1. Optically Thin 10^9 K Pair Plasma

Electron–positron plasma is of significant interest across various fields of physics. For instance, pairs play a crucial role in the dynamics of gamma-ray burst expansion (e.g., [119]) and contributed to the evolution of the early Universe (e.g., [120]). The relevance of pairs has become especially prominent with the availability of high signal-to-noise hard X-ray data from *NuSTAR* [121]: in the hard X-ray band, accreting black holes are observed to radiate significantly above the electron rest mass energy (511 keV, [122]). This high-energy emission above 511 keV is constrained by electron–positron pair production within the compact region of the corona [123], establishing a hard upper limit on coronal temperature relative to the given luminosity. By compiling *NuSTAR* measurements of electron temperatures (kT_e) for a sample of AGN and a few BH X-ray binaries, Fabian et al. [121] found that most sources reside near this hard limit, suggesting pair-dominated coronae in these systems.

Among sources with measurements of kT_e , cool coronae are relatively rare in both AGN and XRBs (e.g., [124–131]). These low- kT_e sources exhibit a wide range of Eddington ratios, from just a few percent [126] to nearly Eddington levels [125]. The inclusion of pair production from non-thermal components within the plasma can account for the observed lower temperatures in these sources [132]. The hybrid plasma model predicts that an increased non-thermal fraction in the corona will lead to a rise in hard X-ray flux and the appearance of the annihilation line, along with a decreasing high-energy cutoff in the spectrum [133].

To demonstrate the effect of a hybrid thermal and non-thermal electron energy distribution, I present the hybrid plasma models for both the hard and soft state spectra of Cyg X-1, using best-fit parameters from Nowak et al. [134] and Gierliński et al. [135] in Figure 3. For simplicity, I only show the disk thermal and coronal emission components. The grey models illustrate the spectral variation when altering the fraction of power supplied to non-thermal particles. Notably, the 511 keV annihilation line is always present but experiences much greater Doppler broadening when the plasma is thermally dominated, allowing for a higher electron temperature.

For Cyg X-1, explaining the observed hard X-ray excess emission of Cyg X-1 solely through pure thermal Comptonisation is challenging (e.g., [136]), a point that has not been fully appreciated: hybrid plasma-based spectral modelling for Cyg X-1 has revealed evidence of a hard X-ray excess above 100 keV, as observed by *Ginga*, *OSSE*, and *COMPTEL* [135,137,138]. Later, the measurements of the electron distribution in the corona of Cyg X-1 were refined with data from GSO, the well-type phoswich counter aboard *Suzaku*, which provided simultaneous hard X-ray data in complement to soft X-ray data from CCD instruments (e.g., [20,134]).

Conducting this type of analysis has proven challenging for several reasons. Markoff et al. [70] proposed that hard X-rays are dominated by inverse Compton scattering at the jet base, with both disk and synchrotron photons serving as seed photons to explain the data. According to this model, the corona at the jet base primarily contributes to hard X-rays, while synchrotron emission dominates from radio through soft X-rays, providing an adequate fit. Nowak et al. [134] tested both the hybrid plasma model and jet models, finding that they work for the hard state up to 300 keV for Cyg X-1. However, constraining these models with the currently available data remains difficult. The future detection of an annihilation line in Cyg X-1 will be crucial for resolving these issues. In the

soft state, when the radio jet is quenched, hard X-ray emission persists, but the flux is too low to obtain a high-quality spectrum for testing the hybrid plasma model. In summary, high-signal-to-noise observations in the hard X-ray to soft gamma-ray range, such as those possible with *COSI* [139], are needed to advance this research.

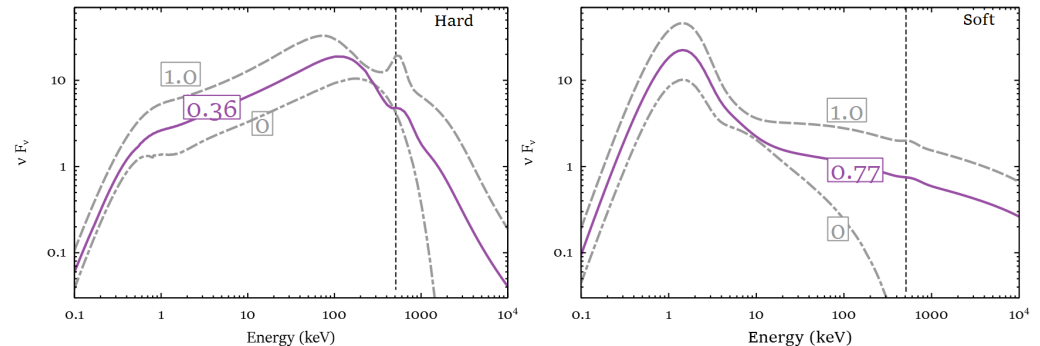


Figure 3. The best-fit hybrid pair plasma models for the coronal emission component of Cyg X-1 in the soft and hard states (in purple). The models were calculated using *Eqpair* [133] based on the best-fit parameters in Nowak et al. [134], Gierliński et al. [135]. The grey models show the spectra for a different fraction of power supplied to the non-thermal distributed particles. Notice the significant increase in hard X-ray emission and the prominent annihilation line at 511 keV when the fraction of non-thermal particles increases. When the non-thermal fraction decreases to zero, this model is consistent with the purely thermal Comptonisation model (e.g., [136]). Note that the annihilation line at 511 keV is still present but only is broadened when the non-thermal fraction is low.

4.2. Optically Thick 10^5 – 10^7 K Plasma

One of the most well-established Eddington-limited analytical accretion models is the standard thin disk model, developed in the 1970s [140] and still widely used today. In this model, the disk is characterised as a geometrically thin, optically thick accretion flow with multi-colour blackbody emission. This model is consistent with the optical and UV emission observed from accreting SMBHs in AGNs and the soft X-ray emission from BH XRBs. To test the standard accretion disk model, one could examine several direct outcomes of this model, such as the geometry of the accretion disk (e.g., [141]) or the estimation of the emission region based on reverberation studies (e.g., [142]).

Spectrally, the standard thin accretion disk model can also be tested using atomic spectra from the accretion disk, with densities predicted by the model. Additionally, the high temperatures and densities of BH accretion disks in strong-gravity environments make them challenging to study in laboratory settings or convincingly simulate computationally. Therefore, X-ray observations of BH accretion disks are unique and crucial for understanding high-energy plasma with extreme properties.

Previous observational studies have explored the relationship between BH mass, mass accretion rates, and the density of the accretion disk in AGNs and XRBs [143,144], which roughly agrees with the expectation in the standard thin disk model. This critical aspect has often been overlooked in the prior research.

Interestingly, an attempt to fit a high-density model to the intermediate state spectra of Cyg X-1 suggested an electron density of approximately 10^{18} cm^{-3} [53]. Compared to a low-density model with an electron density fixed at 10^{15} cm^{-3} , the high-density model² yields a higher reflection strength and implies lower iron abundances. This approach helps address the systematic overestimation of disk iron abundance seen in previous models, though it may not be applicable to all XRB spectra [145].

To further demonstrate the effects of high-density plasma, Figure 4 shows the impact of high density on plasma emission, calculated using the *Reflionx* code [146]. The left panel shows that the disk surface temperature is significantly higher when the electron density is high. This is due to higher heating coefficients (heating rates divided by $n_e n_H$), as in the middle panel. The solid curves represent the heating coefficients due to free-free

absorption (FF), which increase significantly with density, while the dashed curves show the heating coefficients due to recombination cascade (RC). Recombination processes in `Reflionx` have three main components: radiative recombination, three-body recombination, and dielectronic recombination. Radiative recombination occurs when a positively charged ion captures an electron into one of its bound orbits, with simultaneous emission of a photon. In the dielectronic recombination process, the energy released during the capture is used to promote a bound electron to another bound orbit.

At low temperatures, such as deeper into the disk where $\tau > 1$, three-body recombination becomes significant at high densities compared to low densities. An increase in density leads to a rise in the total recombination rate (compare the purple and grey dashed curves in the middle panel). At higher temperatures, such as closer to the disk surface where $\tau < 1$, dielectronic recombination dominates over radiative and three-body recombination. In this regime, the total recombination rate decreases as the density increases. This physical effect, first noted by Burgess and Summers [147], was included in the ion balances of Summers [148] and implemented in `Refionx` by Ross and Fabian [146].

Overall, the resulting spectra are shown in the right panel of Figure 4. The ionisation and density choices in this figure approximate the best-fit parameters for the intermediate state observation of Cyg X-1 [53]. A high-density model exhibits blackbody-like emission in the soft X-ray band due to a higher temperature on the disk surface. Such features have been used to infer disk density from the data in previous studies (e.g., [53,143]). There have also been recent developments in high-density models [149] and attempts in fitting such models to additional objects (e.g., [150–152]). In the context of Cyg X-1, such work still needs further exploration, including investigations into different flux states and the interplay between the disk and the corona.

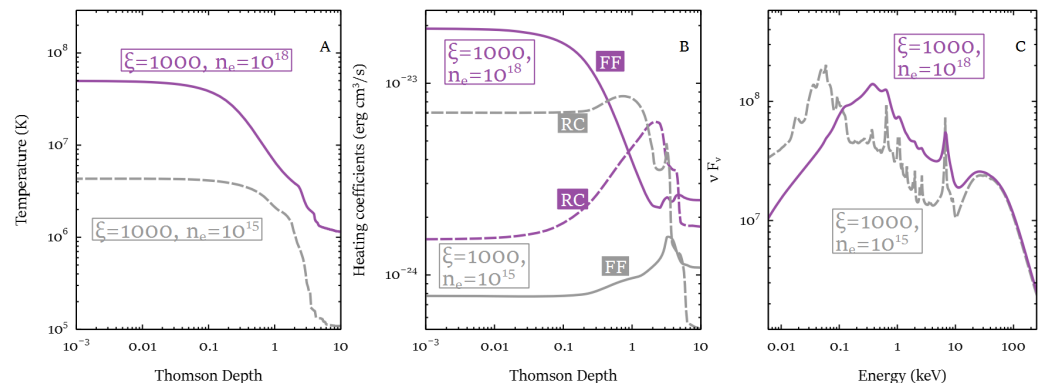


Figure 4. The temperature profiles of a disk with different electron densities are shown in (A) calculated using the codes `Refionx` [146]. At higher densities, the disk surface is significantly hotter due to higher free-free (FF) absorption heating coefficients shown by the solid curves in (B). The dashed curves in the middle panel represent the heating coefficients due to the recombination cascade (RC). In the higher temperature regime (e.g., $\tau < 1$), dielectronic recombination dominates over radiative and three-body recombination. The dielectronic recombination rate decreases with increasing density. In the lower temperature regime (e.g., $\tau > 1$), three-body recombination becomes dominant and increases with density. As the density increases, the dominant heating mechanism shifts from RC to FF, resulting in blackbody-like emission in the spectrum, as shown in (C).

5. Conclusions

In this review, I have summarised some of the most important discoveries related to the BH HMXB Cyg X-1. First, Cyg X-1 stands out as a unique example of a stellar-mass BH. Its young age suggests that the high BH spin inferred from X-ray data is more likely related to its stellar evolution history rather than its accretion history. Moreover, Cyg X-1 differs significantly in terms of mass and BH spin compared to BHs observed through GW detections, implying that they may represent distinct populations of BHs.

Cyg X-1 is also an ideal laboratory for studying accretion physics. Numerous X-ray observations have revealed the presence of an accretion disk that extends close to the innermost stable circular orbit, consistent with the standard thin disk model. However, some open questions remain, such as the origin of the higher-than-expected polarisation degree measured by *IXPE* and the dramatically different polarization angles observed in the hard X-ray to soft gamma-ray band compared to the radio jet orientation by *Integral* and *AstroSAT*. A synergistic effort combining spectral, polarimetric, and timing data is required, and a comprehensive analysis using a consistent model has yet to be completed for Cyg X-1.

Additionally, X-ray observations of Cyg X-1 provide an excellent opportunity to study high-energy plasmas. The detection of hard X-ray emission above 511 keV points to the presence of non-thermal particle distributions, which has not been fully appreciated in current X-ray modelling. This is likely due to the absence of high-energy data, but future missions like *COSI* will be crucial in addressing this gap.

In the soft X-ray band, Cyg X-1 offers the chance to test the standard thin disk model by comparing reflected emission spectra with photoionisation models, based on the expected plasma conditions in the disk. In the intermediate state, the inferred disk density for Cyg X-1 is around a thousand times higher than previously assumed. How this density changes with the spectral state and mass accretion rate remains an open question for future studies.

Funding: J.J. acknowledges support from the Leverhulme Trust, Isaac Newton Trust and St Edmund’s College. J.J. would like to thank the useful discussion with John Tomsick and James Steiner.

Conflicts of Interest: The funders had no role in the design of the study; in the collection, analyses, or interpretation of data; in the writing of the manuscript; or in the decision to publish the results.

Notes

- ¹ In this model, “cold electrons” refers to those with lower Lorentz factors than the bulk Lorentz factor of the jet.
- ² A high density usually refers to values significantly higher than 10^{15} cm^{-3} , which were previously assumed in disk models. For stellar-mass BH accretion disks, high density would range between $10^{18-22} \text{ cm}^{-3}$, while for supermassive BH accretion disks, it usually falls between $10^{15-19} \text{ cm}^{-3}$.

References

1. Bolton, C.T. Identification of Cygnus X-1 with HDE 226868. *Nature* **1972**, *235*, 271–273. [[CrossRef](#)]
2. Webster, B.L.; Murdin, P. Cygnus X-1—a Spectroscopic Binary with a Heavy Companion? *Nature* **1972**, *235*, 37–38. [[CrossRef](#)]
3. Bowyer, S.; Byram, E.T.; Chubb, T.A.; Friedman, H. Cosmic X-ray Sources. *Science* **1965**, *147*, 394–398. [[CrossRef](#)] [[PubMed](#)]
4. Hawking, S. *A Brief History of Time*; Bantam Books: New York, NY, USA, 1998.
5. Orosz, J.A.; McClintock, J.E.; Aufdenberg, J.P.; Remillard, R.A.; Reid, M.J.; Narayan, R.; Gou, L. The Mass of the Black Hole in Cygnus X-1. *Astrophys. J.* **2011**, *742*, 84. [[CrossRef](#)]
6. Miller-Jones, J.C.A.; Bahramian, A.; Orosz, J.A.; Mandel, I.; Gou, L.; Maccarone, T.J.; Neijssel, C.J.; Zhao, X.; Ziółkowski, J.; Reid, M.J.; et al. Cygnus X-1 contains a 21-solar mass black hole—Implications for massive star winds. *Science* **2021**, *371*, 1046–1049. [[CrossRef](#)]
7. Janssens, S.; Shenar, T.; Degenaar, N.; Bodensteiner, J.; Sana, H.; Audenaert, J.; Frost, A.J. MWC 656 is unlikely to contain a black hole. *Astron. Astrophys.* **2023**, *677*, L9. [[CrossRef](#)]
8. Van den Heuvel, E.P.J. High-Mass X-ray Binaries: Progenitors of double compact objects. *Proc. Int. Astron. Union* **2018**, *14*, 1–13. [[CrossRef](#)]
9. Reynolds, C.S. Observing black holes spin. *Nat. Astron.* **2019**, *3*, 41–47. [[CrossRef](#)]
10. Fabian, A.C.; Rees, M.J.; Stella, L.; White, N.E. X-ray fluorescence from the inner disc in Cygnus X-1. *Mon. Not. R. Astron. Soc.* **1989**, *238*, 729–736. [[CrossRef](#)]
11. Reynolds, C.S. Measuring Black Hole Spin Using X-Ray Reflection Spectroscopy. *Space Sci. Rev.* **2014**, *183*, 277–294. [[CrossRef](#)]
12. Zhang, S.N.; Cui, W.; Chen, W. Black Hole Spin in X-Ray Binaries: Observational Consequences. *Astrophys. J. Lett.* **1997**, *482*, L155–L158. [[CrossRef](#)]
13. McClintock, J.E.; Narayan, R.; Steiner, J.F. Black Hole Spin via Continuum Fitting and the Role of Spin in Powering Transient Jets. *Space Sci. Rev.* **2014**, *183*, 295–322. [[CrossRef](#)]
14. Gou, L.; McClintock, J.E.; Remillard, R.A.; Steiner, J.F.; Reid, M.J.; Orosz, J.A.; Narayan, R.; Hanke, M.; García, J. Confirmation via the Continuum-fitting Method that the Spin of the Black Hole in Cygnus X-1 Is Extreme. *Astrophys. J.* **2014**, *790*, 29. [[CrossRef](#)]

15. Kawano, T.; Done, C.; Yamada, S.; Takahashi, H.; Axelsson, M.; Fukazawa, Y. Black hole spin of Cygnus X-1 determined from the softest state ever observed. *Publ. Astron. Soc. Jpn.* **2017**, *69*, 36. [[CrossRef](#)]
16. Zhao, X.; Gou, L.; Dong, Y.; Zheng, X.; Steiner, J.F.; Miller-Jones, J.C.A.; Bahramian, A.; Orosz, J.A.; Feng, Y. Re-estimating the Spin Parameter of the Black Hole in Cygnus X-1. *Astrophys. J.* **2021**, *908*, 117. [[CrossRef](#)]
17. Kushwaha, A.; Agrawal, V.K.; Nandi, A. AstroSat and MAXI view of Cygnus X-1: Signature of an 'extreme' soft nature. *Mon. Not. R. Astron. Soc.* **2021**, *507*, 2602–2613. [[CrossRef](#)]
18. Fabian, A.C.; Wilkins, D.R.; Miller, J.M.; Reis, R.C.; Reynolds, C.S.; Cackett, E.M.; Nowak, M.A.; Pooley, G.G.; Pottschmidt, K.; Sanders, J.S.; et al. On the determination of the spin of the black hole in Cyg X-1 from X-ray reflection spectra. *Mon. Not. R. Astron. Soc.* **2012**, *424*, 217–223. [[CrossRef](#)]
19. Tomsick, J.A.; Nowak, M.A.; Parker, M.; Miller, J.M.; Fabian, A.C.; Harrison, F.A.; Bachetti, M.; Barret, D.; Boggs, S.E.; Christensen, F.E.; et al. The Reflection Component from Cygnus X-1 in the Soft State Measured by NuSTAR and Suzaku. *Astrophys. J.* **2014**, *780*, 78. [[CrossRef](#)]
20. Parker, M.L.; Tomsick, J.A.; Miller, J.M.; Yamaoka, K.; Lohfink, A.; Nowak, M.; Fabian, A.C.; Alston, W.N.; Boggs, S.E.; Christensen, F.E.; et al. NuSTAR and Suzaku Observations of the Hard State in Cygnus X-1: Locating the Inner Accretion Disk. *Astrophys. J.* **2015**, *808*, 9. [[CrossRef](#)]
21. Duro, R.; Dauser, T.; Grinberg, V.; Miškovičová, I.; Rodriguez, J.; Tomsick, J.; Hanke, M.; Pottschmidt, K.; Nowak, M.A.; Kreykenbohm, S.; et al. Revealing the broad iron $K\alpha$ line in Cygnus X-1 through simultaneous XMM-Newton, RXTE, and INTEGRAL observations. *Astron. Astrophys.* **2016**, *589*, A14. [[CrossRef](#)]
22. Walton, D.J.; Tomsick, J.A.; Madsen, K.K.; Grinberg, V.; Barret, D.; Boggs, S.E.; Christensen, F.E.; Clavel, M.; Craig, W.W.; Fabian, A.C.; et al. The Soft State of Cygnus X-1 Observed with NuSTAR: A Variable Corona and a Stable Inner Disk. *Astrophys. J.* **2016**, *826*, 87. [[CrossRef](#)]
23. Krawczynski, H.; Beheshtipour, B. New Constraints on the Spin of the Black Hole Cygnus X-1 and the Physical Properties of its Accretion Disk Corona. *Astrophys. J.* **2022**, *934*, 4. [[CrossRef](#)]
24. Abbott, B.P.; Abbott, R.; Abbott, T.D.; Abernathy, M.R.; Acernese, F.; Ackley, K.; Adams, C.; Adams, T.; Addesso, P.; Adhikari, R.X.; et al. Properties of the Binary Black Hole Merger GW150914. *Phys. Rev. Lett.* **2016**, *116*, 241102. [[CrossRef](#)] [[PubMed](#)]
25. Belczynski, K.; Klencki, J.; Fields, C.E.; Olejak, A.; Berti, E.; Meynet, G.; Fryer, C.L.; Holz, D.E.; O'Shaughnessy, R.; Brown, D.A.; et al. Evolutionary roads leading to low effective spins, high black hole masses, and O1/O2 rates for LIGO/Virgo binary black holes. *Astron. Astrophys.* **2020**, *636*, A104. [[CrossRef](#)]
26. Fishbach, M.; Kalogera, V. Apples and Oranges: Comparing Black Holes in X-Ray Binaries and Gravitational-wave Sources. *Astrophys. J. Lett.* **2022**, *929*, L26. [[CrossRef](#)]
27. Moreno Méndez, E. The need for hypercritical accretion in massive black hole binaries with large Kerr parameters. *Mon. Not. R. Astron. Soc.* **2011**, *413*, 183–189. [[CrossRef](#)]
28. Russell, D.M.; Fender, R.P.; Gallo, E.; Kaiser, C.R. The jet-powered optical nebula of Cygnus X-1. *Mon. Not. R. Astron. Soc.* **2007**, *376*, 1341–1349. [[CrossRef](#)]
29. Zdziarski, A.A.; Chand, S.; Banerjee, S.; Szanecki, M.; Janiuk, A.; Lubinski, P.; Niedzwiecki, A.; Dewangan, G.; Misra, R. What Is the Black Hole Spin in Cyg X-1? *arXiv* **2024**, arXiv:2402.12325. [[CrossRef](#)]
30. Petrucci, P.O.; Gronkiewicz, D.; Rozanska, A.; Belmont, R.; Bianchi, S.; Czerny, B.; Matt, G.; Malzac, J.; Middei, R.; De Rosa, A.; et al. Radiation spectra of warm and optically thick coronae in AGNs. *Astron. Astrophys.* **2020**, *634*, A85. [[CrossRef](#)]
31. Gronkiewicz, D.; Różańska, A.; Petrucci, P.O.; Belmont, R. Thermal instability as a constraint for warm X-ray coronas in active galactic nuclei. *Astron. Astrophys.* **2023**, *675*, A198. [[CrossRef](#)]
32. Neijssel, C.J.; Vinciguerra, S.; Vigna-Gómez, A.; Hirai, R.; Miller-Jones, J.C.A.; Bahramian, A.; Maccarone, T.J.; Mandel, I. Wind Mass-loss Rates of Stripped Stars Inferred from Cygnus X-1. *Astrophys. J.* **2021**, *908*, 118. [[CrossRef](#)]
33. Belczynski, K.; Bulik, T.; Fryer, C.L. High Mass X-ray Binaries: Future Evolution and Fate. *arXiv* **2012**, arXiv:1208.2422. [[CrossRef](#)]
34. Gallegos-Garcia, M.; Fishbach, M.; Kalogera, V.; L Berry, C.P.; Doctor, Z. Do High-spin High-mass X-Ray Binaries Contribute to the Population of Merging Binary Black Holes? *Astrophys. J. Lett.* **2022**, *938*, L19. [[CrossRef](#)]
35. Qin, Y.; Marchant, P.; Fragos, T.; Meynet, G.; Kalogera, V. On the Origin of Black Hole Spin in High-mass X-Ray Binaries. *Astrophys. J. Lett.* **2019**, *870*, L18. [[CrossRef](#)]
36. Shimanskii, V.V.; Karitskaya, E.A.; Bochkarev, N.G.; Galazutdinov, G.A.; Lyuty, V.M.; Shimanskaya, N.N. Analysis of optical spectra of V1357 Cyg \equiv Cyg X-1. *Astron. Rep.* **2012**, *56*, 741–760. [[CrossRef](#)]
37. Batta, A.; Ramirez-Ruiz, E.; Fryer, C. The Formation of Rapidly Rotating Black Holes in High-mass X-Ray Binaries. *Astrophys. J. Lett.* **2017**, *846*, L15. [[CrossRef](#)]
38. Schröder, S.L.; Batta, A.; Ramirez-Ruiz, E. Black Hole Formation in fallback Supernova and the Spins of LIGO Sources. *Astrophys. J. Lett.* **2018**, *862*, L3. [[CrossRef](#)]
39. Abbott, R.; Abbott, T.D.; Acernese, F.; Ackley, K.; Adams, C.; Adhikari, N.; Adhikari, R.X.; Adya, V.B.; Affeldt, C.; Agarwal, D.; et al. Population of Merging Compact Binaries Inferred Using Gravitational Waves through GWTC-3. *Phys. Rev. X* **2023**, *13*, 011048. [[CrossRef](#)]
40. Liotine, C.; Zevin, M.; Berry, C.P.L.; Doctor, Z.; Kalogera, V. The Missing Link between Black Holes in High-mass X-Ray Binaries and Gravitational-wave Sources: Observational Selection Effects. *Astrophys. J.* **2023**, *946*, 4. [[CrossRef](#)]

41. Vink, J.S. Mass loss and the evolution of massive stars. *New Astron. Rev.* **2008**, *52*, 419–422. [[CrossRef](#)]
42. Sukhbold, T.; Ertl, T.; Woosley, S.E.; Brown, J.M.; Janka, H.T. Core-collapse Supernovae from 9 to 120 Solar Masses Based on Neutrino-powered Explosions. *Astrophys. J.* **2016**, *821*, 38. [[CrossRef](#)]
43. Wyrzykowski, L.; Mandel, I. Constraining the masses of microlensing black holes and the mass gap with Gaia DR2. *Astron. Astrophys.* **2020**, *636*, A20. [[CrossRef](#)]
44. Lam, C.Y.; Lu, J.R.; Udalski, A.; Bond, I.; Bennett, D.P.; Skowron, J.; Mróz, P.; Poleski, R.; Sumi, T.; Szymański, M.K.; et al. An Isolated Mass-gap Black Hole or Neutron Star Detected with Astrometric Microlensing. *Astrophys. J. Lett.* **2022**, *933*, L23. [[CrossRef](#)]
45. Lam, C.Y.; Lu, J.R. A Reanalysis of the Isolated Black Hole Candidate OGLE-2011-BLG-0462/MOA-2011-BLG-191. *Astrophys. J.* **2023**, *955*, 116. [[CrossRef](#)]
46. Kaczmarek, Z.; McGill, P.; Perkins, S.E.; Dawson, W.A.; Huston, M.; Ho, M.F.; Abrams, N.S.; Lu, J.R. On Finding Black Holes in Photometric Microlensing Surveys. *arXiv* **2024**, arXiv:2410.14098. [[CrossRef](#)]
47. Hurlley, J.R.; Pols, O.R.; Tout, C.A. Comprehensive analytic formulae for stellar evolution as a function of mass and metallicity. *Mon. Not. R. Astron. Soc.* **2000**, *315*, 543–569. [[CrossRef](#)]
48. Belczynski, K.; Taam, R.E.; Kalogera, V.; Rasio, F.A.; Bulik, T. On the Rarity of Double Black Hole Binaries: Consequences for Gravitational Wave Detection. *Astrophys. J.* **2007**, *662*, 504–511. [[CrossRef](#)]
49. Belczynski, K.; Dominik, M.; Bulik, T.; O’Shaughnessy, R.; Fryer, C.; Holz, D.E. The Effect of Metallicity on the Detection Prospects for Gravitational Waves. *Astrophys. J. Lett.* **2010**, *715*, L138–L141. [[CrossRef](#)]
50. Gaia Collaboration; Panuzzo, P.; Mazeh, T.; Arenou, F.; Holl, B.; Caffau, E.; Jorissen, A.; Babusiaux, C.; Gavras, P.; Sahlmann, J.; et al. Discovery of a dormant 33 solar-mass black hole in pre-release Gaia astrometry. *Astron. Astrophys.* **2024**, *686*, L2. [[CrossRef](#)]
51. Tananbaum, H.; Gursky, H.; Kellogg, E.; Giacconi, R.; Jones, C. Observation of a Correlated X-Ray Transition in Cygnus X-1. *Astrophys. J. Lett.* **1972**, *177*, L5. [[CrossRef](#)]
52. Grinberg, V.; Hell, N.; Pottschmidt, K.; Böck, M.; Nowak, M.A.; Rodriguez, J.; Bodaghee, A.; Cadolle Bel, M.; Case, G.L.; Hanke, M.; et al. Long term variability of Cygnus X-1. V. State definitions with all sky monitors. *Astron. Astrophys.* **2013**, *554*, A88. [[CrossRef](#)]
53. Tomsick, J.A.; Parker, M.L.; García, J.A.; Yamaoka, K.; Barret, D.; Chiu, J.L.; Clavel, M.; Fabian, A.; Fürst, F.; Gandhi, P.; et al. Alternative Explanations for Extreme Supersolar Iron Abundances Inferred from the Energy Spectrum of Cygnus X-1. *Astrophys. J.* **2018**, *855*, 3. [[CrossRef](#)]
54. König, O.; Mastroserio, G.; Dauser, T.; Méndez, M.; Wang, J.; García, J.A.; Steiner, J.F.; Pottschmidt, K.; Ballhausen, R.; Connors, R.M.; et al. Long term variability of Cygnus X-1. VIII. A spectral-timing look at low energies with NICER. *Astron. Astrophys.* **2024**, *687*, A284. [[CrossRef](#)]
55. Kong, A.K.H.; McClintock, J.E.; Garcia, M.R.; Murray, S.S.; Barret, D. The X-Ray Spectra of Black Hole X-Ray Novae in Quiescence as Measured by Chandra. *Astrophys. J.* **2002**, *570*, 277–286. [[CrossRef](#)]
56. Yuan, F.; Narayan, R. Hot Accretion Flows Around Black Holes. *Annu. Rev. Astron. Astrophys.* **2014**, *52*, 529–588. [[CrossRef](#)]
57. Plant, D.S.; Fender, R.P.; Ponti, G.; Muñoz-Darias, T.; Coriat, M. The truncated and evolving inner accretion disc of the black hole GX 339-4. *Astron. Astrophys.* **2015**, *573*, A120. [[CrossRef](#)]
58. Garcia, J.A.; Steiner, J.F.; McClintock, J.E.; Remillard, R.A.; Grinberg, V.; Dauser, T. X-Ray Reflection Spectroscopy of the Black Hole GX 339-4: Exploring the Hard State with Unprecedented Sensitivity. *Astrophys. J.* **2015**, *813*, 84. [[CrossRef](#)]
59. Xrism Collaboration; Audard, M.; Awaki, H.; Ballhausen, R.; Bamba, A.; Behar, E.; Boissay-Malaquin, R.; Brenneman, L.; Brown, G.V.; Corrales, L.; et al. XRISM Spectroscopy of the Fe K α Emission Line in the Seyfert Active Galactic Nucleus NGC 4151 Reveals the Disk, Broad-line Region, and Torus. *Astrophys. J. Lett.* **2024**, *973*, L25. [[CrossRef](#)]
60. XRISM Collaboration. The XRISM/Resolve view of the Fe K region of Cyg X-3. *arXiv* **2024**, arXiv:2411.00597. [[CrossRef](#)]
61. Thorne, K.S.; Price, R.H. Cygnus X-1: An interpretation of the spectrum and its variability. *Astrophys. J. Lett.* **1975**, *195*, L101–L105. [[CrossRef](#)]
62. Sunyaev, R.A.; Truemper, J. Hard X-ray spectrum of CYG X-1. *Nature* **1979**, *279*, 506–508. [[CrossRef](#)]
63. Fabian, A.C.; Zoghbi, A.; Ross, R.R.; Uttley, P.; Gallo, L.C.; Brandt, W.N.; Blustin, A.J.; Boller, T.; Caballero-Garcia, M.D.; Larsson, J.; et al. Broad line emission from iron K- and L-shell transitions in the active galaxy 1H0707-495. *Nature* **2009**, *459*, 540–542. [[CrossRef](#)] [[PubMed](#)]
64. Kara, E.; Steiner, J.F.; Fabian, A.C.; Cackett, E.M.; Uttley, P.; Remillard, R.A.; Gendreau, K.C.; Arzoumanian, Z.; Altamirano, D.; Eikenberry, S.; et al. The corona contracts in a black-hole transient. *Nature* **2019**, *565*, 198–201. [[CrossRef](#)] [[PubMed](#)]
65. Reis, R.C.; Miller, J.M.; Reynolds, M.T.; Fabian, A.C.; Walton, D.J.; Cackett, E.; Steiner, J.F. Evidence of Light-bending Effects and Its Implication for Spectral State Transitions. *Astrophys. J.* **2013**, *763*, 48. [[CrossRef](#)]
66. Chartas, G.; Rhea, C.; Kochanek, C.; Dai, X.; Morgan, C.; Blackburne, J.; Chen, B.; Mosquera, A.; MacLeod, C. Gravitational lensing size scales for quasars. *Astron. Nachrichten* **2016**, *337*, 356. [[CrossRef](#)]
67. Wilkins, D.R.; Fabian, A.C. Understanding X-ray reflection emissivity profiles in AGN: Locating the X-ray source. *Mon. Not. R. Astron. Soc.* **2012**, *424*, 1284–1296. [[CrossRef](#)]
68. Henri, G.; Petrucci, P.O. Anisotropic illumination of AGN’s accretion disk by a non thermal source. I. General theory and application to the Newtonian geometry. *Astron. Astrophys.* **1997**, *326*, 87–98. [[CrossRef](#)]

69. Miniutti, G.; Fabian, A.C.; Goyder, R.; Lasenby, A.N. The lack of variability of the iron line in MCG-6-30-15: General relativistic effects. *Mon. Not. R. Astron. Soc.* **2003**, *344*, L22–L26. [[CrossRef](#)]
70. Markoff, S.; Nowak, M.A.; Wilms, J. Going with the Flow: Can the Base of Jets Subsume the Role of Compact Accretion Disk Coronae? *Astrophys. J.* **2005**, *635*, 1203–1216. [[CrossRef](#)]
71. Gonzalez, A.G.; Wilkins, D.R.; Gallo, L.C. Probing the geometry and motion of AGN coronae through accretion disc emissivity profiles. *Mon. Not. R. Astron. Soc.* **2017**, *472*, 1932–1945. [[CrossRef](#)]
72. Galeev, A.A.; Rosner, R.; Vaiana, G.S. Structured coronae of accretion disks. *Astrophys. J.* **1979**, *229*, 318–326. [[CrossRef](#)]
73. Stern, B.E.; Poutanen, J.; Svensson, R.; Sikora, M.; Begelman, M.C. On the Geometry of the X-Ray–Emitting Region in Seyfert Galaxies. *Astrophys. J. Lett.* **1995**, *449*, L13. [[CrossRef](#)]
74. Eardley, D.M.; Lightman, A.P.; Shapiro, S.L. Cygnus X-1: A two-temperature accretion disk model which explains the observed hard X-ray spectrum. *Astrophys. J. Lett.* **1975**, *199*, L153–L155. [[CrossRef](#)]
75. Krawczynski, H.; Muleri, F.; Dovčiak, M.; Veledina, A.; Rodriguez Cavero, N.; Svoboda, J.; Ingram, A.; Matt, G.; Garcia, J.A.; Loktev, V.; et al. Polarized x-rays constrain the disk-jet geometry in the black hole x-ray binary Cygnus X-1. *Science* **2022**, *378*, 650–654. [[CrossRef](#)] [[PubMed](#)]
76. Gallo, E.; Fender, R.; Kaiser, C.; Russell, D.; Morganti, R.; Oosterloo, T.; Heinz, S. A dark jet dominates the power output of the stellar black hole Cygnus X-1. *Nature* **2005**, *436*, 819–821. [[CrossRef](#)]
77. Poutanen, J.; Veledina, A.; Beloborodov, A.M. Polarized X-Rays from Windy Accretion in Cygnus X-1. *Astrophys. J. Lett.* **2023**, *949*, L10. [[CrossRef](#)]
78. Beloborodov, A.M. Electron-positron outflows from gamma-ray emitting accretion discs. *Mon. Not. R. Astron. Soc.* **1999**, *305*, 181–189. [[CrossRef](#)]
79. Dauser, T.; García, J.; Wilms, J. Relativistic reflection: Review and recent developments in modeling. *Astron. Nachrichten* **2016**, *337*, 362. [[CrossRef](#)]
80. You, B.; Tuo, Y.; Li, C.; Wang, W.; Zhang, S.N.; Zhang, S.; Ge, M.; Luo, C.; Liu, B.; Yuan, W.; et al. Insight-HXMT observations of jet-like corona in a black hole X-ray binary MAXI J1820+070. *Nat. Commun.* **2021**, *12*, 1025. [[CrossRef](#)]
81. Liu, B.F.; Mineshige, S.; Shibata, K. A Simple Model for a Magnetic Reconnection-heated Corona. *Astrophys. J. Lett.* **2002**, *572*, L173–L176. [[CrossRef](#)]
82. Miller, K.A.; Stone, J.M. The Formation and Structure of a Strongly Magnetized Corona above a Weakly Magnetized Accretion Disk. *Astrophys. J.* **2000**, *534*, 398–419. [[CrossRef](#)]
83. Dexter, J.; Begelman, M.C. A relativistic outflow model of the X-ray polarization in Cyg X-1. *Mon. Not. R. Astron. Soc.* **2024**, *528*, L157–L160. [[CrossRef](#)]
84. Begelman, M.C.; Sikora, M. Inverse Compton Scattering of Ambient Radiation by a Cold Relativistic Jet: A Source of Beamed, Polarized X-Ray and Optical Observations of X-Ray–selected BL Lacertae Objects. *Astrophys. J.* **1987**, *322*, 650. [[CrossRef](#)]
85. Rodriguez, J.; Grinberg, V.; Laurent, P.; Cadolle Bel, M.; Pottschmidt, K.; Pooley, G.; Bodaghee, A.; Wilms, J.; Gouiffès, C. Spectral State Dependence of the 0.4–2 MeV Polarized Emission in Cygnus X-1 Seen with INTEGRAL/IBIS, and Links with the AMI Radio Data. *Astrophys. J.* **2015**, *807*, 17. [[CrossRef](#)]
86. Russell, D.M.; Shahbaz, T. The multiwavelength polarization of Cygnus X-1. *Mon. Not. R. Astron. Soc.* **2014**, *438*, 2083–2096. [[CrossRef](#)]
87. Jourdain, E.; Roques, J.P.; Chauvin, M.; Clark, D.J. Separation of Two Contributions to the High Energy Emission of Cygnus X-1: Polarization Measurements with INTEGRAL SPI. *Astrophys. J.* **2012**, *761*, 27. [[CrossRef](#)]
88. Fender, R.P.; Stirling, A.M.; Spencer, R.E.; Brown, I.; Pooley, G.G.; Muxlow, T.W.B.; Miller-Jones, J.C.A. A transient relativistic radio jet from Cygnus X-1. *Mon. Not. R. Astron. Soc.* **2006**, *369*, 603–607. [[CrossRef](#)]
89. Chattopadhyay, T.; Kumar, A.; Rao, A.R.; Bhargava, Y.; Vadawale, S.V.; Ratheesh, A.; Dewangan, G.; Bhattacharya, D.; Mithun, N.P.S.; Bhalerao, V. High Hard X-Ray Polarization in Cygnus X-1 Confined to the Intermediate Hard State: Evidence for a Variable Jet Component. *Astrophys. J. Lett.* **2024**, *960*, L2. [[CrossRef](#)]
90. Bouchet, T.; Rodriguez, J.; Cangemi, F.; Thalhhammer, P.; Laurent, P.; Grinberg, V.; Wilms, J.; Pottschmidt, K. INTEGRAL/IBIS polarization detection in the hard and soft intermediate states of Swift J1727.8–1613. *Astron. Astrophys.* **2024**, *688*, L5. [[CrossRef](#)]
91. Steiner, J.F.; Nathan, E.; Hu, K.; Krawczynski, H.; Dovčiak, M.; Veledina, A.; Muleri, F.; Svoboda, J.; Alabarta, K.; Parra, M.; et al. An IXPE-led X-Ray Spectropolarimetric Campaign on the Soft State of Cygnus X-1: X-Ray Polarimetric Evidence for Strong Gravitational Lensing. *Astrophys. J. Lett.* **2024**, *969*, L30. [[CrossRef](#)]
92. Jana, A.; Chang, H.K. X-ray polarization changes with the state transition in Cygnus X-1. *Mon. Not. R. Astron. Soc.* **2024**, *527*, 10837–10843. [[CrossRef](#)]
93. Ratheesh, A.; Dovčiak, M.; Krawczynski, H.; Podgorný, J.; Marra, L.; Veledina, A.; Suleimanov, V.F.; Rodriguez Cavero, N.; Steiner, J.F.; Svoboda, J.; et al. X-Ray Polarization of the Black Hole X-Ray Binary 4U 1630–47 Challenges the Standard Thin Accretion Disk Scenario. *Astrophys. J.* **2024**, *964*, 77. [[CrossRef](#)]
94. Rodriguez Cavero, N.; Marra, L.; Krawczynski, H.; Dovčiak, M.; Bianchi, S.; Steiner, J.F.; Svoboda, J.; Capitanio, F.; Matt, G.; Negro, M.; et al. The First X-Ray Polarization Observation of the Black Hole X-Ray Binary 4U 1630–47 in the Steep Power-law State. *Astrophys. J. Lett.* **2023**, *958*, L8. [[CrossRef](#)]

95. Podgorný, J.; Marra, L.; Muleri, F.; Rodriguez Cavero, N.; Ratheesh, A.; Dovčiak, M.; Mikušincová, R.; Brigitte, M.; Steiner, J.F.; Veledina, A.; et al. The first X-ray polarimetric observation of the black hole binary LMC X-1. *Mon. Not. R. Astron. Soc.* **2023**, *526*, 5964–5975. [[CrossRef](#)]
96. Marra, L.; Brigitte, M.; Rodriguez Cavero, N.; Chun, S.; Steiner, J.F.; Dovčiak, M.; Nowak, M.; Bianchi, S.; Capitanio, F.; Ingram, A.; et al. IXPE observation confirms a high spin in the accreting black hole 4U 1957+115. *Astron. Astrophys.* **2024**, *684*, A95. [[CrossRef](#)]
97. Svoboda, J.; Dovčiak, M.; Steiner, J.F.; Kaaret, P.; Podgorný, J.; Poutanen, J.; Veledina, A.; Muleri, F.; Taverna, R.; Krawczynski, H.; et al. Dramatic Drop in the X-Ray Polarization of Swift J1727.8–1613 in the Soft Spectral State. *Astrophys. J. Lett.* **2024**, *966*, L35. [[CrossRef](#)]
98. Chandrasekhar, S. *Radiative Transfer*; Dover Publication: Mineola, NY, USA, 1960.
99. Straub, O.; Bursa, M.; Sądowski, A.; Steiner, J.F.; Abramowicz, M.A.; Kluźniak, W.; McClintock, J.E.; Narayan, R.; Remillard, R.A. Testing slim-disk models on the thermal spectra of LMC X-3. *Astron. Astrophys.* **2011**, *533*, A67. [[CrossRef](#)]
100. Fabian, A.C.; Buisson, D.J.; Kosec, P.; Reynolds, C.S.; Wilkins, D.R.; Tomsick, J.A.; Walton, D.J.; Gandhi, P.; Altamirano, D.; Arzoumanian, Z.; et al. The soft state of the black hole transient source MAXI J1820+070: Emission from the edge of the plunge region? *Mon. Not. R. Astron. Soc.* **2020**, *493*, 5389–5396. [[CrossRef](#)]
101. Nowak, M.A. Are there three peaks in the power spectra of GX 339-4 and Cyg X-1? *Mon. Not. R. Astron. Soc.* **2000**, *318*, 361–367. [[CrossRef](#)]
102. Pottschmidt, K.; Wilms, J.; Nowak, M.A.; Pooley, G.G.; Gleissner, T.; Heindl, W.A.; Smith, D.M.; Remillard, R.; Staubert, R. Long term variability of Cygnus X-1. I. X-ray spectral-temporal correlations in the hard state. *Astron. Astrophys.* **2003**, *407*, 1039–1058. [[CrossRef](#)]
103. Axelsson, M.; Done, C. Breaking the spectral degeneracies in black hole binaries with fast timing data: The hard state of Cygnus X-1. *Mon. Not. R. Astron. Soc.* **2018**, *480*, 751–758. [[CrossRef](#)]
104. Uttley, P.; McHardy, I.M.; Vaughan, S. Non-linear X-ray variability in X-ray binaries and active galaxies. *Mon. Not. R. Astron. Soc.* **2005**, *359*, 345–362. [[CrossRef](#)]
105. Gierliński, M.; Zdziarski, A.A. Discovery of powerful millisecond flares from Cygnus X-1. *Mon. Not. R. Astron. Soc.* **2003**, *343*, L84–L88. [[CrossRef](#)]
106. Grinberg, V.; Pottschmidt, K.; Böck, M.; Schmid, C.; Nowak, M.A.; Uttley, P.; Tomsick, J.A.; Rodriguez, J.; Hell, N.; Markowitz, A.; et al. Long term variability of Cygnus X-1. VI. Energy-resolved X-ray variability 1999–2011. *Astron. Astrophys.* **2014**, *565*, A1. [[CrossRef](#)]
107. Zhou, M.; Grinberg, V.; Bu, Q.C.; Santangelo, A.; Cangemi, F.; Diez, C.M.; König, O.; Ji, L.; Nowak, M.A.; Pottschmidt, K.; et al. The spectral-timing analysis of Cygnus X-1 with Insight-HXMT. *Astron. Astrophys.* **2022**, *666*, A172. [[CrossRef](#)]
108. Cui, W.; Heindl, W.A.; Rothschild, R.E.; Zhang, S.N.; Jahoda, K.; Focke, W. Rossi X-Ray Timing Explorer Observation of Cygnus X-1 in Its High State. *Astrophys. J. Lett.* **1997**, *474*, L57–L60. [[CrossRef](#)]
109. Li, Y.; Yan, Z.; Gao, C.; Yu, W. X-ray spectral and timing evolution during the 2018 outburst of MAXI J1820+070. *arXiv* **2024**, arXiv:2407.08421. [[CrossRef](#)]
110. Uttley, P.; McHardy, I.M. The flux-dependent amplitude of broadband noise variability in X-ray binaries and active galaxies. *Mon. Not. R. Astron. Soc.* **2001**, *323*, L26–L30. [[CrossRef](#)]
111. Gaskell, C.M. Lognormal X-Ray Flux Variations in an Extreme Narrow-Line Seyfert 1 Galaxy. *Astrophys. J. Lett.* **2004**, *612*, L21–L24. [[CrossRef](#)]
112. Gleissner, T.; Wilms, J.; Pottschmidt, K.; Uttley, P.; Nowak, M.A.; Staubert, R. Long term variability of Cyg X-1. II. The rms-flux relation. *Astron. Astrophys.* **2004**, *414*, 1091–1104. [[CrossRef](#)]
113. Wilms, J.; Nowak, M.A.; Pottschmidt, K.; Pooley, G.G.; Fritz, S. Long term variability of Cygnus X-1. IV. Spectral evolution 1999–2004. *Astron. Astrophys.* **2006**, *447*, 245–261. [[CrossRef](#)]
114. Lyubarskii, Y.E. Flicker noise in accretion discs. *Mon. Not. R. Astron. Soc.* **1997**, *292*, 679–685. [[CrossRef](#)]
115. Arévalo, P.; Uttley, P. Investigating a fluctuating-accretion model for the spectral-timing properties of accreting black hole systems. *Mon. Not. R. Astron. Soc.* **2006**, *367*, 801–814. [[CrossRef](#)]
116. Mastroserio, G.; Ingram, A.; van der Klis, M. An X-ray reverberation mass measurement of Cygnus X-1. *Mon. Not. R. Astron. Soc.* **2019**, *488*, 348–361. [[CrossRef](#)]
117. Uttley, P.; Wilkinson, T.; Cassatella, P.; Wilms, J.; Pottschmidt, K.; Hanke, M.; Böck, M. The causal connection between disc and power-law variability in hard state black hole X-ray binaries. *Mon. Not. R. Astron. Soc.* **2011**, *414*, L60–L64. [[CrossRef](#)]
118. Wang, J.; Mastroserio, G.; Kara, E.; García, J.A.; Ingram, A.; Connors, R.; van der Klis, M.; Dauser, T.; Steiner, J.F.; Buisson, D.J.K.; et al. Disk, Corona, Jet Connection in the Intermediate State of MAXI J1820+070 Revealed by NICER Spectral-timing Analysis. *Astrophys. J. Lett.* **2021**, *910*, L3. [[CrossRef](#)]
119. Goodman, J. Are gamma-ray bursts optically thick? *Astrophys. J. Lett.* **1986**, *308*, L47. [[CrossRef](#)]
120. Kolb, E.W.; Turner, M.S. *The Early Universe*; Addison-Wesley Publishing: Boston, MA, USA, 1990; Volume 69.
121. Fabian, A.C.; Lohfink, A.; Kara, E.; Parker, M.L.; Vasudevan, R.; Reynolds, C.S. Properties of AGN coronae in the NuSTAR era. *Mon. Not. R. Astron. Soc.* **2015**, *451*, 4375–4383. [[CrossRef](#)]
122. Guilbert, P.W.; Fabian, A.C.; Rees, M.J. Spectral and variability constraints on compact sources. *Mon. Not. R. Astron. Soc.* **1983**, *205*, 593–603. [[CrossRef](#)]

123. Svensson, R. Electron-Positron Pair Equilibria in Relativistic Plasmas. *Astrophys. J.* **1982**, *258*, 335. [[CrossRef](#)]
124. Tazaki, F.; Ueda, Y.; Ishino, Y.; Eguchi, S.; Isobe, N.; Terashima, Y.; Mushotzky, R.F. Suzaku Observation of the Brightest Broad-line Radio Galaxy 4C 50.55 (IGR J21247+5058). *Astrophys. J.* **2010**, *721*, 1340–1347. [[CrossRef](#)]
125. Kara, E.; García, J.A.; Lohfink, A.; Fabian, A.C.; Reynolds, C.S.; Tombesi, F.; Wilkins, D.R. The high-Eddington NLS1 Ark 564 has the coolest corona. *Mon. Not. R. Astron. Soc.* **2017**, *468*, 3489–3498. [[CrossRef](#)]
126. Tortosa, A.; Marinucci, A.; Matt, G.; Bianchi, S.; La Franca, F.; Ballantyne, D.R.; Boorman, P.G.; Fabian, A.C.; Farrah, D.; Fuerst, F.; et al. Broad-band X-ray spectral analysis of the Seyfert 1 galaxy GRS 1734-292. *Mon. Not. R. Astron. Soc.* **2017**, *466*, 4193–4200. [[CrossRef](#)]
127. Walton, D.J.; Brightman, M.; Risaliti, G.; Fabian, A.C.; Fürst, F.; Harrison, F.A.; Lohfink, A.; Matt, G.; Miniutti, G.; Parker, M.L.; et al. Disentangling the complex broad-band X-ray spectrum of IRAS 13197-1627 with NuSTAR, XMM-Newton and Suzaku. *Mon. Not. R. Astron. Soc.* **2018**, *473*, 4377–4391. [[CrossRef](#)]
128. Xu, Y.; Harrison, F.A.; García, J.A.; Fabian, A.C.; Fürst, F.; Gandhi, P.; Grefenstette, B.W.; Madsen, K.K.; Miller, J.M.; Parker, M.L.; et al. Reflection Spectra of the Black Hole Binary Candidate MAXI J1535-571 in the Hard State Observed by NuSTAR. *Astrophys. J. Lett.* **2018**, *852*, L34. [[CrossRef](#)]
129. Jiang, J.; Walton, D.J.; Fabian, A.C.; Parker, M.L. A relativistic disc reflection model for 1H0419-577: Multi-epoch spectral analysis with XMM-Newton and NuSTAR. *Mon. Not. R. Astron. Soc.* **2019**, *483*, 2958–2967. [[CrossRef](#)]
130. Buisson, D.J.K.; Fabian, A.C.; Barret, D.; Fürst, F.; Gandhi, P.; García, J.A.; Kara, E.; Madsen, K.K.; Miller, J.M.; Parker, M.L.; et al. MAXI J1820+070 with NuSTAR I. An increase in variability frequency but a stable reflection spectrum: Coronal properties and implications for the inner disc in black hole binaries. *Mon. Not. R. Astron. Soc.* **2019**, *490*, 1350–1362. [[CrossRef](#)]
131. Zhang, Z.; Jiang, J.; Liu, H.; Bambi, C.; Reynolds, C.S.; Fabian, A.C.; Dauser, T.; Madsen, K.; Young, A.; Gallo, L.; et al. The Low Temperature Corona in ESO 511—G030 Revealed by NuSTAR and XMM-Newton. *arXiv* **2022**, arXiv:2208.01452. [[CrossRef](#)]
132. Fabian, A.C.; Lohfink, A.; Belmont, R.; Malzac, J.; Coppi, P. Properties of AGN coronae in the NuSTAR era—II. Hybrid plasma. *Mon. Not. R. Astron. Soc.* **2017**, *467*, 2566–2570. [[CrossRef](#)]
133. Coppi, P.S. The Physics of Hybrid Thermal/Non-Thermal Plasmas. *arXiv* **1999**, arXiv:astro-ph/9903158. [[CrossRef](#)]
134. Nowak, M.A.; Hanke, M.; Trowbridge, S.N.; Markoff, S.B.; Wilms, J.; Pottschmidt, K.; Coppi, P.; Maitra, D.; Davis, J.E.; Trammer, F. Corona, Jet, and Relativistic Line Models for Suzaku/RXTE/Chandra-HETG Observations of the Cygnus X-1 Hard State. *Astrophys. J.* **2011**, *728*, 13. [[CrossRef](#)]
135. Gierliński, M.; Zdziarski, A.A.; Poutanen, J.; Coppi, P.S.; Ebisawa, K.; Johnson, W.N. Radiation mechanisms and geometry of Cygnus X-1 in the soft state. *Mon. Not. R. Astron. Soc.* **1999**, *309*, 496–512. [[CrossRef](#)]
136. Titarchuk, L. Generalized Comptonization Models and Application to the Recent High-Energy Observations. *Astrophys. J.* **1994**, *434*, 570. [[CrossRef](#)]
137. Ling, J.C.; Mahoney, W.A.; Wheaton, W.A.; Jacobson, A.S. Long-Term Gamma-Ray Spectral Variability of Cygnus X-1. *Astrophys. J. Lett.* **1987**, *321*, L117. [[CrossRef](#)]
138. Poutanen, J.; Coppi, P.S. Unification of Spectral States of Accreting Black Holes. In Proceedings of the 19th Texas Symposium on Relativistic Astrophysics and Cosmology, Paris, France, 14–18 December 1998; p. 355.
139. Tomsick, J.A.; Boggs, S.E.; Zoglauer, A.; Hartmann, D.; Ajello, M.; Burns, E.; Fryer, C.; Karwin, C.; Kierans, C.; Lowell, A.; et al. The Compton Spectrometer and Imager. *arXiv* **2023**, arXiv:2308.12362. [[CrossRef](#)]
140. Shakura, N.I.; Sunyaev, R.A. Black holes in binary systems. Observational appearance. *Astron. Astrophys.* **1973**, *24*, 337–355.
141. Jiang, J.; Abdikamalov, A.B.; Bambi, C.; Reynolds, C.S. Black hole spin measurements based on a thin disc model with finite thickness - I. An example study of MCG-06-30-15. *Mon. Not. R. Astron. Soc.* **2022**, *514*, 3246–3259. [[CrossRef](#)]
142. Kammoun, E.S.; Papadakis, I.E.; Dovčiak, M. A Hard Look at Thermal Reverberation and Optical/Ultraviolet Lags in NGC 5548. *Astrophys. J. Lett.* **2019**, *879*, L24. [[CrossRef](#)]
143. Jiang, J.; Fabian, A.C.; Wang, J.; Walton, D.J.; García, J.A.; Parker, M.L.; Steiner, J.F.; Tomsick, J.A. High-density reflection spectroscopy: I. A case study of GX 339-4. *Mon. Not. R. Astron. Soc.* **2019**, *484*, 1972–1982. [[CrossRef](#)]
144. Jiang, J.; Fabian, A.C.; Dauser, T.; Gallo, L.; García, J.A.; Kara, E.; Parker, M.L.; Tomsick, J.A.; Walton, D.J.; Reynolds, C.S. High Density Reflection Spectroscopy - II. The density of the inner black hole accretion disc in AGN. *Mon. Not. R. Astron. Soc.* **2019**, *489*, 3436–3455. [[CrossRef](#)]
145. Liu, H.; Jiang, J.; Zhang, Z.; Bambi, C.; Fabian, A.C.; García, J.A.; Ingram, A.; Kara, E.; Steiner, J.F.; Tomsick, J.A.; et al. High-density Reflection Spectroscopy of Black Hole X-Ray Binaries in the Hard State. *Astrophys. J.* **2023**, *951*, 145. [[CrossRef](#)]
146. Ross, R.R.; Fabian, A.C. X-ray reflection in accreting stellar-mass black hole systems. *Mon. Not. R. Astron. Soc.* **2007**, *381*, 1697–1701. [[CrossRef](#)]
147. Burgess, A.; Summers, H.P. The Effects of Electron and Radiation Density on Dielectronic Recombination. *Astrophys. J.* **1969**, *157*, 1007. [[CrossRef](#)]
148. Summers, H.P. The ionization equilibrium of hydrogen-like to argon-like ions of elements. *Mon. Not. R. Astron. Soc.* **1974**, *169*, 663–680. [[CrossRef](#)]
149. Ding, Y.; García, J.A.; Kallman, T.R.; Mendoza, C.; Bautista, M.; Harrison, F.A.; Tomsick, J.A.; Dong, J. Next Generation Accretion Disk Reflection Model: High-Density Plasma Effects. *arXiv* **2024**, arXiv:2409.00253. [[CrossRef](#)]
150. Jiang, J.; Buisson, D.J.K.; Dauser, T.; Fabian, A.C.; Fürst, F.; Gallo, L.C.; Harrison, F.A.; Parker, M.L.; Steiner, J.F.; Tomsick, J.A.; et al. A NuSTAR and Swift view of the hard state of MAXI J1813-095. *Mon. Not. R. Astron. Soc.* **2022**, *514*, 1952–1960. [[CrossRef](#)]

151. Connors, R.M.T.; García, J.A.; Tomsick, J.; Mastroserio, G.; Grinberg, V.; Steiner, J.F.; Jiang, J.; Fabian, A.C.; Parker, M.L.; Harrison, F.; et al. The Long-stable Hard State of XTE J1752-223 and the Disk Truncation Dilemma. *Astrophys. J.* **2022**, *935*, 118. [[CrossRef](#)]
152. Coughenour, B.M.; Tomsick, J.A.; Mastroserio, G.; Steiner, J.F.; Connors, R.M.T.; Jiang, J.; Hare, J.; Shaw, A.W.; Ludlam, R.M.; Fabian, A.C.; et al. Reflection and Timing Study of the Transient Black Hole X-Ray Binary MAXI J1803-298 with NuSTAR. *Astrophys. J.* **2023**, *949*, 70. [[CrossRef](#)]

Disclaimer/Publisher's Note: The statements, opinions and data contained in all publications are solely those of the individual author(s) and contributor(s) and not of MDPI and/or the editor(s). MDPI and/or the editor(s) disclaim responsibility for any injury to people or property resulting from any ideas, methods, instructions or products referred to in the content.